

Application of portable FTIR spectrometers for detecting greenhouse gas emissions of the megacity Berlin

F. Hase(1), M. Frey(1), T. Blumenstock(1), J. Groß(1), M. Kiel(1), R. Kohlhepp(2), G. Mengistu Tsidu(1,4), K. Schäfer(3), M. K. Sha(1), and J. Orphal(1)

(1) Karlsruhe Institute of Technology (KIT), Institute for Meteorology and Climate Research (IMK-ASF), Karlsruhe, Germany

(2) German Weather Service, Offenbach, Germany

(3) Karlsruhe Institute of Technology (KIT), Institute for Meteorology and Climate Research (IMK-IFU), Garmisch-Partenkirchen, Germany

(4) Department of Physics, Addis Ababa University, P.O. Box: 1176, Addis Ababa, Ethiopia

Correspondence to: Frank Hase (frank.hase@kit.edu)

Abstract

Five portable Bruker EM27/SUN FTIR (Fourier Transform InfraRed) spectrometers have been used for the accurate and precise observation of column-averaged abundances of CO₂ and CH₄ around the megacity Berlin. In the work by Frey et al., 2015, a calibration procedure is developed and applied to the set of spectrometers used for the Berlin campaign. Here, we describe the observational setup of the campaign and aspects of the data analysis, and we present the recorded time series of XCH₄ and XCO₂. We demonstrate that the CO₂ emissions of Berlin can be clearly identified in the observations. A simple dispersion model is applied which indicates a total strength of the Berlin source of about 0.8 tons of CO₂ per second. In the electronic supplement of this work, we provide the measured dataset and auxiliary data. We hope that the model community will exploit this unique dataset for state-of-the art inversion studies of CO₂ and CH₄ sources in the Berlin area.

1 Introduction

The application of portable FTIR (Fourier Transform InfraRed) spectrometers for the observation of column-averaged CO₂ and CH₄ abundances holds great promises with respect to the quantification of sources and sinks of greenhouse gases on regional and smaller scales. Although in-situ measurements at the ground can be performed with unrivaled precision and accuracy, these measurements suffer from the fact that they detect local variations and so are heavily influenced by local contributions and by details of the vertical mixing. Use of in-situ measurements on different altitude levels (tall tower, aircraft) improves the representativeness considerably, but is a rather expensive approach. Current space-based remote sensing observations are useful for the quantification of sources and sinks on continental scales, but still suffer from limited precision, limited density of observations, and biases related to details of atmospheric scattering properties. Ground-based observations using high-resolution laboratory spectrometers as performed by TCCON (Total Carbon Column Observing Network, Wunch et al., 2011) can provide column-averaged abundances with reference precision and accuracy, but the number of sites is limited and the stations are not mobile. Portable FTIR spectrometers therefore are a very promising complement to current techniques, because they can probe larger sample volumes than in-situ and smaller scales than current space-based sensors or globally distributed ground-based remote sensing networks. In this work, we demonstrate the approach of using solar absorption spectra recorded with small low-resolution FTIR spectrometers at several sites distributed around a source region for an estimation of the encircled source strength.

The demonstration is based on a campaign we performed from June, 23, 2014 to July, 11, 2014 around Berlin using five spectrometers. We decided to target Berlin for several reasons. Firstly, Berlin is a megacity, so we expect to measure detectable enhancements. Secondly, the city is relatively isolated, so that CO₂ emissions really can be attributed to Berlin. Thirdly, the flat topography is favorable, which supports the interpretation of the recorded data. Measurements were performed at five different stations around Berlin, four of them roughly located along a circle with a radius of 12 km around the city centre of Berlin. One instrument was positioned inside the Berlin motorway ring in Charlottenburg, somewhat closer to the city centre than the other instruments. A map with all sites is shown in figure 1. The coordinates and altitudes of the different stations are displayed in table 1. Due to somewhat unfavourable

weather conditions, we were able to perform simultaneous measurements at all sites only on 10 days during the demonstration campaign. However, it should be noted that such spectrometers can be installed for longer periods of operation in weather-resistant shelters and operated automatically – in order to form a permanent component of future monitoring systems.

Due to the long lifetimes of CO₂ and CH₄, each individual source contribution is a weak signal superimposed on the average column-averaged background abundance. Therefore, ensuring a common calibration of all involved spectrometers and demonstrating their instrumental stability is of utmost importance for the proposed method. In Frey et al., 2015, a rigorous calibration procedure for the EM27/SUN spectrometer is developed and is exemplified using the set of portable spectrometers which we used for the Berlin campaign. This calibration procedure involved pre- and after campaign measurements, thereby proving unambiguously the excellent instrumental stability of the devices.

2 Observational setup, weather, prevailing winds and auxiliary measurements

Each site was equipped with an EM27/SUN spectrometer including a solar tracker, a GPS sensor used for accurate timekeeping, and a MHB-382SD data logger for recording pressure, temperature and relative humidity. The measurement procedures (scan speed, resolution, numerical apodisation, etc) applied during the campaign were chosen identical to those applied for the calibration measurements.

In table 2, we collect the main characteristics of each measurement day. We list the number of observations available at each site, and deduce a daily quality flag according to the overall data availability. Furthermore, the wind speeds and prevailing wind directions in the boundary layer are provided. The best measurement days with measurements throughout most of the day (solar elevation angle > 20 deg) were June, 27, July, 3, and July, 4. During these days, prevailing winds were from the West (and South). Wind speeds were moderate in the range of five to eight knots. Note that although not very well covered, the set of observations includes

1 a Sunday (July, 6), which is an interesting aspect, as a different temporal pattern and overall
2 strength of emissions is expected on a Sunday than during a working day.

3
4 Very important auxiliary information required for the proper estimation of a source strength is
5 the development of the boundary layer height during each day of observations. IMK-IFU
6 performed continuous ceilometer measurements of the boundary layer height during the
7 whole campaign period. The measurements were performed in Berlin Neukölln (52.4895 N,
8 13.4309 E), 2.5 km to the southeast of the city center. The ceilometer CL51 from Vaisala
9 GmbH, Hamburg, Germany, is an eye-safe commercial mini-lidar system. Ceilometers detect
10 initially the cloud height, but special software provides routine retrievals of up to five lifted
11 layers from vertical profiles (vertical gradient) of laser backscatter density data (Münel,
12 2007). In the absence of low clouds and precipitation and during scattered clouds, this
13 measurement method estimates boundary layer height fairly well. The CL51 detects
14 convective layer depths exceeding 2000 m and nocturnal stable layers down to 50 m. The
15 measurement results agree well with those which are determined from profiles of relative
16 humidity and virtual potential temperature measured by radiosonde (location of strong height
17 gradient of aerosol backscatter density and relative humidity as well as temperature inversion,
18 see Emeis et al. , 2012). But radiosondes which are launched routinely twice per day only do
19 not provide sufficient information. Figure 2 shows the ceilometer results for June, 27: the
20 developing boundary layer can be clearly seen, reaching an altitude of about 2200 m in the
21 late afternoon. In the case of airborne particles it has been shown previously that boundary
22 layer information as detected continuously by ceilometers enables the determination of near-
23 surface concentrations from column density data (Schäfer et al., 2008).

24 25 **3 The XH_2O , XCO_2 and XCH_4 time series**

26 The analysis of the trace gases from the measured spectra has been performed as described by
27 Gisi et al., 2012, and Frey et al., 2015. Because the distances between the sites are about 25
28 km or less, a common pressure-temperature profile has been used for the analysis at all sites.
29 The pressure records of the MHB-382SD devices have been used to set the ground pressure
30 values of the model atmosphere, and an intraday variability of the ground pressure and the
31 temperature profile has been taken into account in the analysis of the spectra. For the
32 construction of the temperature profiles, we utilize the NCEP model noon profiles provided

1 by the Goddard automailer system and radiosonde data provided by the meteorological
2 observatory Lindenberg. We take the NCEP data as the starting values and overlap a linear
3 ascent during the day, which is the temperature difference between the 12 am and 6 pm sonde
4 data, for the lowermost height levels (below 4 km altitude). For the height levels above 4 km
5 we take the original NCEP noon data, as the change during the day is negligible.

6
7 Solar absorption spectral observations in the near infrared offer the potential of measuring
8 column-averaged dry air mole fractions with excellent precision and accuracy. This is owed to
9 the facts that (1) scattering of photons into the line-of-sight is a negligible process and that (2)
10 absorption bands of molecular oxygen are covered, so the column amount of oxygen can be
11 derived from the same spectrum. Because the dry air mole fraction of molecular oxygen is
12 nearly invariable, the column-averaged dry air mole fraction of the target gases can be derived
13 from the ratio of the observed target gas columns and the oxygen column. This approach
14 significantly reduces the impact of various error sources on the final results, because these
15 typically affect both the target gas columns and the oxygen reference column (Wunch et al.,
16 2011). Moreover, the amount of dry air deduced from the spectral information can be
17 compared with the ground pressure measured with a barometer. Note that the barometer
18 records the total ground pressure including the pressure exerted by the water vapour column.
19 However, this small contribution to the pressure can be taken into account in the comparison,
20 because the water vapour column can also be derived from the observed spectrum. Figure 3
21 shows the time series of the total ground pressure (derived from the average of the continuous
22 barometer measurements performed with the MHB-382SD devices at all five sites) in
23 comparison to the total ground pressures calculated from the spectral measurements (taking
24 into account the water vapour contribution). The pressure values from the spectral
25 measurements follow closely the variable ground pressure and the agreement between
26 different stations is excellent. A least squares fit to the barometer data suggests a common
27 calibration factor of 0.9713 for the spectroscopic measurements, which has been applied in
28 the figure. This result is in excellent agreement with the calibration factor found by Frey et
29 al., 2015 (0.9700) and Klappenbach et al., 2015 (0.9717).

30
31 Figure 4 (top panel) shows the observed time series of H₂O dry air mole fractions. As
32 expected, H₂O varies considerably - by about a factor of three - over the campaign period. On

1 the other hand, the agreement between the stations is surprisingly good. This demonstrates the
2 uniform character of the selected area, especially the absence of localized dominating sources
3 of atmospheric humidity, which would induce larger differences between the stations. Finally,
4 as the main contribution to the H_2O total column originates from the boundary layer, this
5 finding supports the assumption that the boundary layer across the whole probed area is well
6 ventilated.

7
8 Figure 4 (middle and bottom panel) shows the XCO_2 and XCH_4 values, respectively, as
9 observed by all spectrometers. The dominating synoptic variations which are common to all
10 sites occur on timescales of several days. These variations on the order of one per cent peak-
11 to-peak are due to the changing tropopause altitude and advection of air masses with different
12 trace gas concentrations. In addition, the time series reveal intraday variability on the order of
13 0.5 % or less, which is variable from day to day, but also very similar in each individual data
14 record. We assume that these variations result from a superposition of real variability and
15 artefacts of the retrieval. During most of the observation days, a decrease of XCO_2 is found,
16 which is what would be expected as a result of photosynthetic activity during a sunny day
17 (high insulation being an obvious selection bias of solar absorption observations). On the
18 other hand, variations symmetric around noon are particularly striking during a couple of
19 days, mainly in the case of CH_4 . It is plausible to assume an airmass-dependent retrieval bias
20 as a cause of these variations. We detailed in the first part of this work that we attempted to
21 remove this artefact by applying an a-posteriori airmass-dependent correction. However, the
22 observed bias is comprised of two contributions: one contribution resulting from forward
23 model errors (e.g. wrong line broadening parameters) - this tends to be a systematic feature
24 and can be removed by the global correction we applied - and a second contribution due to the
25 smoothing error of the retrieval. The column sensitivity of the scaling retrieval is a function of
26 airmass, and so is the smoothing error. As described in the first part of this work, we used
27 constant a-priori profile shapes in the retrievals, while the actual atmospheric profiles are
28 variable. This gives rise to airmass-dependent artefacts which are variable from day to day.
29 Finally, on top of this variable background, subtle differences between individual
30 observations can be detected: these are typically of the order of 1 to 2 per mil and it is
31 tempting to assume that these are caused by local emission contributions. For illustration,
32 figure 5 shows the XCH_4 and XCO_2 values observed during June, 27. Southerly winds

1 prevailed during that day, and indeed the XCO_2 values observed in Heiligensee in the
2 Northwest of Berlin are elevated. It is important to note that although the emission signals
3 tend to be smaller than the observed intraday variability, enhancements as small as 0.5 per mil
4 are noticeable. This is possible because the detection of an enhancement can be based on the
5 differences between the column-averaged mole fractions observed at different sites, if these
6 are superimposed on a smoothly varying background traced by the observations of several
7 upstream stations. This situation is realized if all sites observe similar advected larger scale
8 variations. Note that at a given time during the day all sites perform measurements under
9 nearly the same solar elevation angle and quite similar atmospheric conditions (atmospheric
10 vertical profile shapes of trace gases). This reduces significantly retrieval biases between the
11 stations, especially if the interpretation of the collected data is mainly based on differences
12 between simultaneous observations of upstream and downstream stations. In detail, the
13 observed XCH_4 enhancements differ from the XCO_2 enhancements, which is expected due to
14 different sources. Moreover, the background of the XCH_4 seems less well defined and more
15 variable. This meets the expectation: due to the likely presence of rural CH_4 sources around
16 the conurbation area encircled with the stations and due to the stronger contrast between
17 tropospheric and stratospheric mixing ratios of CH_4 higher variability is expected in the XCH_4
18 background field than in case of XCO_2 . We feel that a sensible investigation of our XCH_4
19 observations would require a state-of-the-art high-resolution inversion model and we hope
20 that the datasets made available in the electronic supplement of this work will be exploited in
21 depth by the inverse model community. Using a simple dispersion model, we will in the
22 following focus on a more specific interpretation of the observed XCO_2 enhancements. In the
23 next section, we describe the main characteristics of the dispersion model. In section 5 we
24 compare observations and model predictions.

27 **4 Setup of a simple dispersion model**

28 For a prediction of the differences in XCO_2 between sites we have created a simple dispersion
29 model. Within this modelling scheme, the Berlin source is mapped into a schematic area
30 source spanned by five neighbouring rectangles, which contribute to the total source strength.
31 The central rectangle reflects the city center, the four remaining rectangles reflect
32 Charlottenburg and Spandau areas (western box), Reinickendorf and Pankau areas (northern

box), Marzahn-Hellersdorf and Treptow-Köpenick areas (eastern / south-eastern box), and the Tempelhof-Schöneberg area (southern box). The geographical coordinates of each box and the percentage contribution to the total emission are listed in table 3. The spatial extent and contribution of each box have been adjusted according to information on population and traffic density provided by the bureau of statistics of Berlin-Brandenburg (<http://www.stadtentwicklung.berlin.de>).

The dispersion model uses analysed hourly horizontal wind fields from COSMO-DE, the convective-scale regional component of the numerical weather prediction system of the German Weather Service DWD (Baldauf et al., 2011). Due to the fact that we assume a distributed source region, we do not apply the COSMO wind field at full resolution, which is on the order of 2.8 x 2.8 km, but use only five COSMO hourly wind profiles distributed over the observation area (in the center and the NW, NE, SW, SE corners of a square centered on Berlin with an edge length of about 20 km) and interpolate the winds between these reference wind profiles linearly along time and - assuming a Shepard inverse distance weighting with a power of two (Shepard, 1968) - in a horizontal plane.

The model is based on a strict Lagrangian perspective. It does not use a model grid, but instead transports emitted particles according to the interpolated winds at their current locations. The generation rate of the particles is proportional to the source strength, they are created at the ground level within one of the five emission regions described before. For each creation act, the region is selected by a random generator in accordance with the assumed contribution of the region, the starting position within the selected area is again chosen randomly. Within a selected region, the probability of emission is equal for each area element; we do not attempt to resolve sources on a scale smaller than the source region.

Concerning the vertical transport, a fast mixing on timescales of ~10 minutes across the whole boundary layer is assumed. This is realized in the model by introducing a fast erratic diffusion of each “molecule” along the vertical axis. The altitude limit of the model boundary layer is for each day chosen in accordance with ceilometer measurements. Fast fluctuations of the boundary layer thickness detected by the ceilometer are neglected, instead the individual

overall development of the boundary layer height during each day is approximated using piecewise linear fits.

Finally, the detection of particles is emulated by checking whether the “molecule” is inside a cylinder which wraps the line of sight of one of the observation sites. It should be noted that due to the daily apparent motion of the sun in the sky, the position of this cylinder is quite variable. If we assume a boundary layer thickness of 1500 m and start and end of observations at a solar elevation angle of 20 degree, then the top surface of the cylinder is shifted by 8 km westwards during the day, which is not negligible in comparison to the extent of the assumed source regions. Therefore, the line-of-sight used for the detection condition is updated in the model according to the astronomical conditions.

The simulation period starts at midnight. In each time step (1 sec), a “molecule” is emitted and all existing particles are transported. During daytime, as long as the solar elevation exceeds 20°, the number of detected particles at each observation site is determined in intervals of 450 sec. Typically, depending on wind speed, 20 000 to 40 000 particles are traced at a given time (each emitted “molecule” is followed for up to a distance of 40 km from the Berlin center). The simulation run for each day is repeated 500 times and the results averaged to achieve a negligible statistical noise in the number of detection counts. Note that the model does not take into account emissions from the previous day. Typically, these aged emissions have left the region of interest before, but occasionally - if the wind speed is very low - it might happen that they reside for longer than 6 hours in the observed area, or may return from outside the modelled area if the wind direction is changing. No attempt is made in the dispersion calculation to include the variable advected XCO₂ background, it only predicts the enhancements at each observation site due to the daily emissions of the local Berlin source.

5 Comparison of predicted and observed time series

In the following, we compare the XCO₂ measurements with results from the dispersion model for the three most favourable observation days. For all days, the Berlin CO₂ source strength was fixed to a plausible value of 800 kg CO₂ per second. The source strength was kept

constant during the day, although one would certainly expect considerable intraday variability for different kinds of contributions, e.g. traffic peaking at around 8 am and 5 pm (local time). Figures 6 to 8 show the observational and model results for June, 27, July, 3, and July, 4. For the first two days, the model enhancements are shown superimposed on a smooth polynomial background, which is reasonably well defined by the observations of the upstream stations. During the third day, July, 4, it is more difficult to estimate a smooth background level, as all stations, including the upstream stations, observe considerable variability. Therefore, for this day the predicted enhancements are shown superimposed on a constant 390 ppm background level.

The model prediction for June, 27, is of acceptable quality. The enhancements before noon observed first in Charlottenburg and afterwards in Heiligensee are well captured. The peak at 0.35 day fraction observed in Heiligensee, is much sharper than the model prediction and indicates a significant contribution of a localised source smaller than the assumed emission regions. Southerly winds prevailed during the day, so this source is probably located in model region 1. Indeed, the heat and power generating coal-fired plant Reuter West operated by Vattenfall AB with a peak thermal power of 774 MW (Ref: <http://kraftwerke.vattenfall.de/powerplant/reuter-west>) is located in this region and is the likely source of the observed emissions. Afterwards, the model predicts elevated values for Heiligensee until around noon, which is in good agreement with the observations, but it fails to predict the final enhancement observed in Heiligensee after noontime.

For July, 3, the enhancements are smaller than those observed during June, 27. Still, the undulations predicted by the model are detectable in the Lindenberg time series reasonably well, although the first two peaks are underestimated and appear delayed in the model simulation by about half an hour. The final increase towards the third peak observed in the afternoon is nicely reproduced. The model predicts slightly higher values for Mahlsdorf than for Heiligensee and Lichtenrade, which is not supported by the observations, which instead indicate repeated peaks in the Heiligensee and Lichtenrade timeseries. Westerly winds were prevailing during that day, so for the station Lichtenrade emissions from Potsdam (not included in the model) are likely to contribute.

For July, 4, the observed XCO₂ values are quite variable. An M-shaped disturbance extending over five hours and observed at all stations before noon is most prominent feature. Southerly winds prevailed near ground and southwesterly winds in the free troposphere. While a similar shape is observed at all stations, there is a clear time lag of about 45 minutes between the occurrence of this disturbance between the upstream stations (Lichtenrade and Charlottenburg) and the downstream stations (Heiligensee and Lindenberg). This time lag agrees well with the delay expected for the advection of a disturbance in the background XCO₂ signal at a wind speed of about 7 m/s across a distance of about 20 km between the sites. The variations between the stations are too strong to allow a judgement concerning the model prediction of a 0.5 ppm enhancement at Heiligensee and Charlottenburg.

Figure 9 shows the MACC (Monitoring Atmospheric Composition & Climate project) prediction for XCO₂. A closer examination of the previous development of the XCO₂ field according to MACC indicates that the complex structures in the XCO₂ field around Berlin during that day are possibly the result of an entrainment of emissions from Western Germany and further sources nearer to Berlin. The example of July, 4, demonstrates the limitations of a simple dispersion model which takes into account only the local sources. A comprehensive exploitation of the information contained in the kind of measurements presented here would require state-of-the-art inverse modelling allowing for a resolved local source distribution nested into a much wider model area. Such a model configuration would include a reasonable description of variations due to advected XCO₂ contributions from outside the model area and associated larger-scale variations of column-averaged abundances.

6 Dataset provided in the Supplement

In the electronic supplement of this work, we provide the complete set of quality-filtered XCH₄ and XCO₂ observations collected during the campaign at all stations. The quality filter is based on the quality of the interferograms (average value and fluctuation of the DC value). For each site, we provide the apparent solar elevation angle of the measurement, the retrieved total column amount of H₂O and the XCH₄ and XCO₂ calibrated with respect to TCCON and corrected for the systematic spurious air mass dependence (column-averaged dry air mole fractions in ppm). In separate tables, we provide the a-priori profile shapes of CH₄ and CO₂ used for the scaling retrieval on the 49 model levels of the retrieval code (dry air mole

fractions in ppm) and the averaging kernel matrices of dimension 49 x 49 for different solar zenith angles. These auxiliary data enable the user to estimate the smoothing error of the column-averaged abundances, especially the impact of the actual profile shape on XCH₄ and XCO₂. If the user wants to include the smoothing characteristics of the remote sensing observations in the comparison between observations and assimilation model we suggest including the kernel convolution directly in the model predictor. In addition to the FTIR data, the electronic supplement contains the results derived from the ceilometer observations in both tabulated and graphical form.

7 Summary and Outlook

We presented measurements of column-averaged abundances of CH₄ and CO₂ recorded with five portable FTIR spectrometers during a measurement campaign of three weeks duration around Berlin in summer 2014. The results demonstrate that an array of well-calibrated, ground-based FTIR spectrometers allow the reliable detection of XCH₄ and XCO₂ enhancements due to local emissions in the range of one per mil. Application of a simple dispersion model indicates that the observations are compatible with an assumed source strength on the order of 800 kg CO₂ /s for the megacity Berlin. We believe that arrays formed with such spectrometers would be a very useful complement to existing in-situ and remote-sensing measurements for the quantification of sources and sinks of CH₄ and CO₂ on regional scales. We expect that a comprehensive inversion of local source contributions to the observed column-averaged abundances will require state-of-the art nested model approaches which include a proper description of the variable advected background contributions. Such model studies could also be of great value for the design of monitoring networks (density and locations of stations) based on portable FTIR spectrometers.

Acknowledgements

We acknowledge support by the ACROSS research infrastructure of the Helmholtz Association.

1 We thank the National Center for Environmental Prediction (NCEP) for providing
2 atmospheric temperature profiles via the Goddard Auto mailer system.

3
4 We acknowledge the availability of XCO₂ maps from MACC-III. MACC-III is a
5 Coordination & Support Action (2014-2015) funded by the European Union under the
6 Horizon 2020 Programme, coordinated by the European Centre for Medium-Range Weather
7 Forecasts and operated by a 36-member consortium. Further project details can be found at
8 <http://www.gmes-atmosphere.eu>. Andre Butz, KIT, kindly prepared the plot based on MACC-
9 III data.

10
11 We are very thankful for the successful cooperation during the measurement campaign
12 “Berlin Air quality and Ecosystem Research: Local and long-range Impact of anthropogenic
13 and Natural hydrocarbons” (BAERLIN2014), and especially the coordinators Boris Bonn and
14 Erika von Schneidemesser, Institute for Advanced Sustainability Studies e.V., Potsdam,
15 Germany.

16
17 We thank the German Weather Service (DWD) for providing the COSMO-DE analysis data
18 which were used for the wind profiles in the dispersion model.

19
20 We acknowledge support by Deutsche Forschungsgemeinschaft and Open Access Publishing
21 Fund of the Karlsruhe Institute of Technology.

References

- Baldauf, M., A. Seifert, J. Förstner, D. Majewski, M. Raschendorfer, T. Reinhardt: Operational Convective-Scale Numerical Weather Prediction with the COSMO Model: Description and Sensitivities, *Mon. Wea. Rev.*, 139/12, 3887-3905, 2011, doi: 10.1175/MWR-D-10-05013.1.
- Emeis, S., Schäfer, K., Munkel, C., Friedl, R., and Suppan, P.: Evaluation of the interpretation of ceilometer data with RASS and radiosonde data, *Bound-Lay. Meteorol.*, 143, 25–35, 2012.
- Frey, M., F. Hase, T. Blumenstock, J. Groß, M. Kumar Sha, M. Kiel, R. Kohlhepp, G. Mengistu Tsidu, K. Schäfer, and J. Orphal: Calibration and instrumental line shape characterisation of a set of portable FTIR spectrometers for detecting greenhouse gas emissions, submitted to AMTD, 2015.
- Gisi, M., Hase, F., Dohe, S., Blumenstock, T., Simon, A., and Keens, A.: XCO₂-measurements with a tabletop FTS using solar absorption spectroscopy, *Atmospheric Measurement Techniques*, 5, 2969–2980, doi:10.5194/amt-5-2969-2012, 2012.
- Klappenbach, F., M. Bertle, J. Kostinek, F. Hase, T. Blumenstock, A. Agusti-Panareda, M. Razinger and A. Butz: Accurate mobile remote sensing of XCO₂ and XCH₄ latitudinal transects from aboard a research vessel, submitted to AMTD, 2015.
- Munkel, C.: Mixing height determination with lidar ceilometers - results from Helsinki Testbed, *Meteorol. Z.*, 16, 451-459, 2007.
- Schäfer, K., Harbusch, A., Emeis, S., Koepke, P., and Wiegner, M.: Correlation of aerosol mass near the ground with aerosol optical depth during two seasons in Munich. *Atmos. Environ.*, 42, 18, 4036-4046, 2008.
- Shepard, D.: Proceedings of the 1968 ACM National Conference. pp. 517–524, 1968, doi:10.1145/800186.810616.
- Wunch, D., G.C. Toon, J.-F.L. Blavier, R.A. Washenfelder, J. Notholt, B.J. Connor, D.W.T. Griffith, V. Sherlock, P.O. Wennberg. The Total Carbon Column Observing Network. *Phil. Trans. R. Soc. A*, 2011, 369, doi:10.1098/rsta.2010.0240.

1

site	latitude [°]	longitude [° E]	altitude [m]
Mahlsdorf	52.486	13.589	39.0
Charlottenburg	52.505	13.302	47.7
Heiligensee	52.622	13.228	34.5
Lindenberg	52.601	13.519	63.3
Lichtenrade	52.391	13.392	44.8

2

3 Table 1. Geographical coordinates and altitudes of the measurement sites around Berlin. The
4 coordinates were derived using GPS sensors. The reported altitudes result from combining
5 time-averaged GPS measurements which were repeatedly performed at Mahlsdorf and
6 average differences between the time series of ground pressures recorded at each site.
7 Excellent agreement with topographic data provided on the website <http://www.wieweit.net>
8 are found.

9

date JJMMDD	# observations					quality	wind speed (m/s)	wind direction
140626 (Th)	76	70	89	28	116	+	1 ... 2	NNE
140627 (Fr)	273	233	237	186	182	+++	2.5	SSW ... SSE
140628 (Sa)	0	37	0	0	0	o	3.5	SSW
140701 (Tu)	203	189	158	122	224	++	4	W
140702 (We)	106	128	92	76	129	+	4.5	W
140703 (Th)	316	358	320	354	357	+++	3.5	W
140704 (Fr)	545	509	545	652	511	++++	3.5	SW ... S
140705 (Sa)	0	93	0	0	0	o	2.5	SSW ... SSE
140706 (Su)	329	265	346	252	385	++	2.5	W ... SW
140707 (Mo)	10	74	28	98	130	+	4	SE ... NW
140708 (Tu)	0	21	0	0	0	o	3	NE ... E
140709 (We)	35	29	40	0	10	o	3 ... 5	E ... SSW
140710	248	306	411	188	245	++	3...6...3	NE ... E

(Th)								
140711 (Fr)	257	248	212	243	253	+	4	NE

1

2

3 Table 2. Summary of all measurement days: number of observations at each site (Mahlsdorf,
4 Charlottenburg, Heiligensee, Lindenberg, Lichtenrade), overall quality ranking of each day
5 according to number of available observations and temporal coverage, ground wind speed and
6 direction (classification from poor to excellent: o, +, ++, +++, ++++).

1

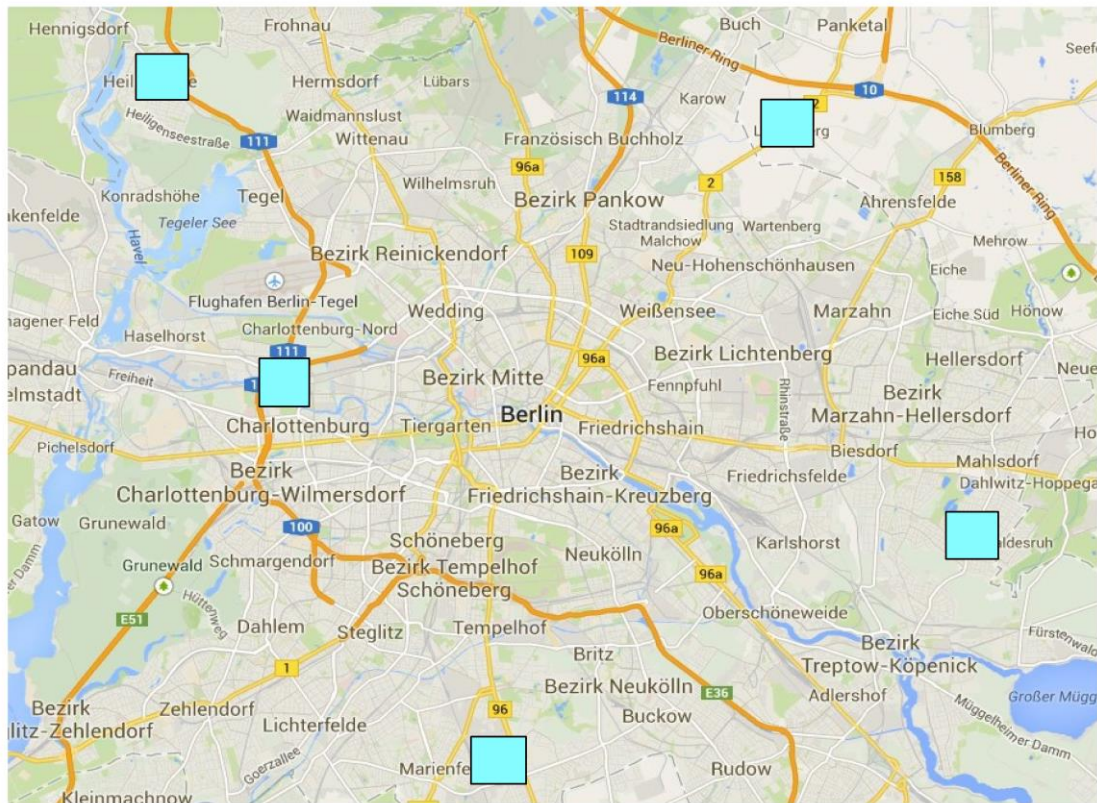
Box ID	area	NW corner	SE corner	% contribution
1	Charlottenburg and Spandau	52.5677 13.0753	52.5159 13.2550	25
2	Tempelhof-Schöneberg	52.4657 13.2304	52.3800 13.4275	15
3	Marzahn-Hellersdorf and Treptow-Köpenick	52.5531 13.4502	52.3927 13.6316	10
4	Reinickendorf and Pankau	52.6302 13.3046	52.5472 13.4721	10
5	city center	52.5472 13.2550	52.4657 13.4502	40

2

3 Table 3. The five emission regions used in the dispersion model. The last row provides the
4 percentage contribution to the total emission strength of the Berlin source as assumed in the
5 model.

6

7



1

2 Figure 1. Map showing the measurement stations around Berlin

3

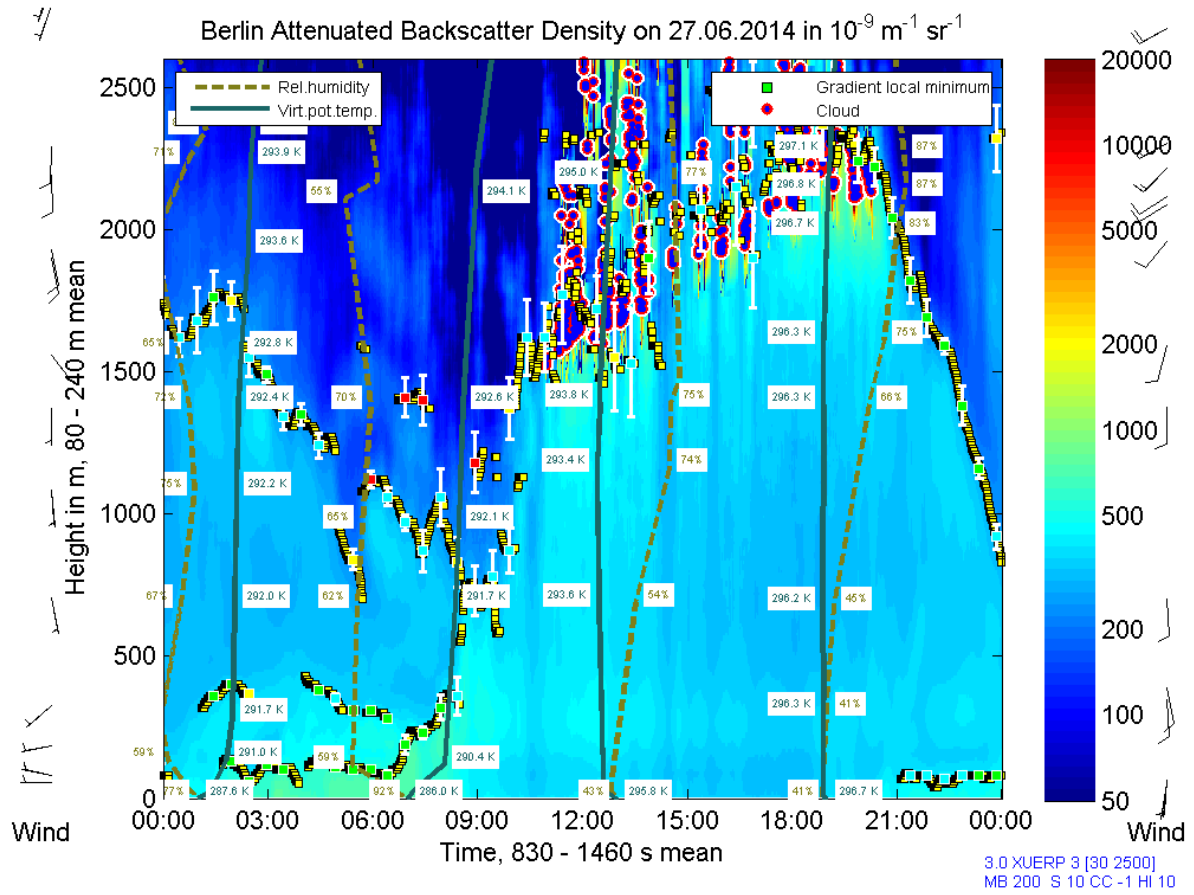


Figure 2. The development of the boundary layer thickness during June, 27 according to ceilometer measurements performed by IMK-IFU in Berlin-Neukölln.

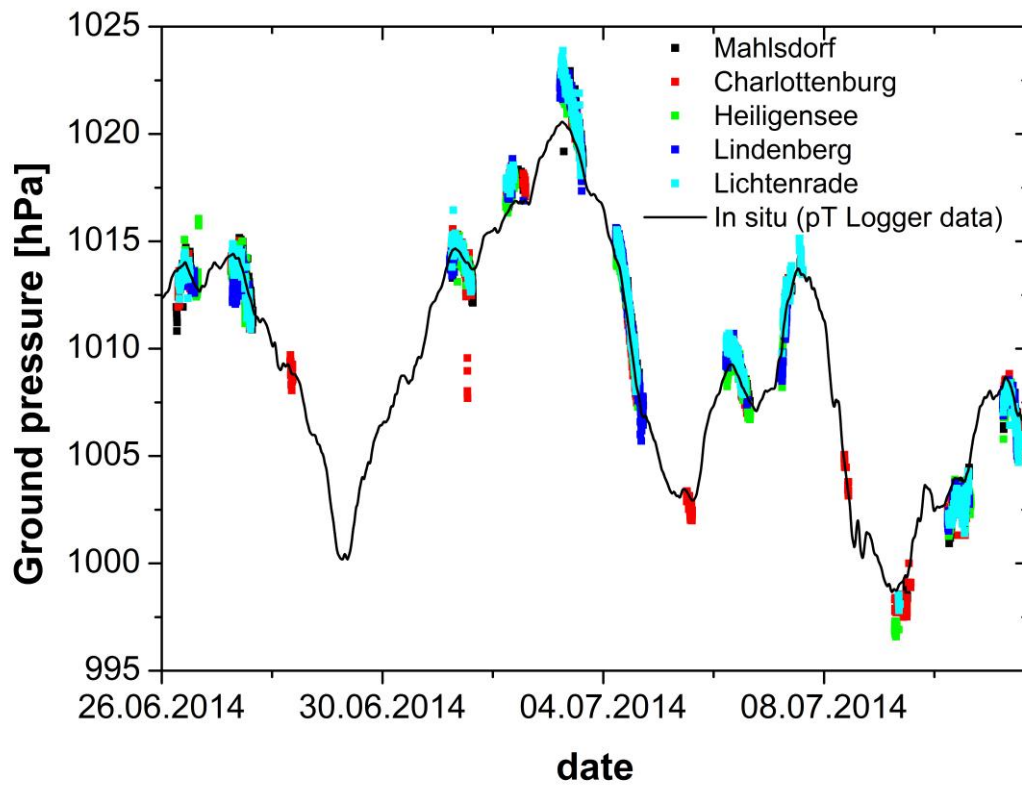


Figure 3. Time series of ground pressure according to the barometer measurements performed at each site (black line) and derived from the infrared spectra (dots). All pressure values were reduced to a common reference altitude of 30 m. For the spectroscopic results, the dry ground pressure has been derived from the 1.27 μm oxygen band and the contribution of water vapour to the total ground pressure has been taken into account. In order to achieve the best agreement with the barometer results, a calibration factor of 0.9713 has been applied to the spectroscopic results.

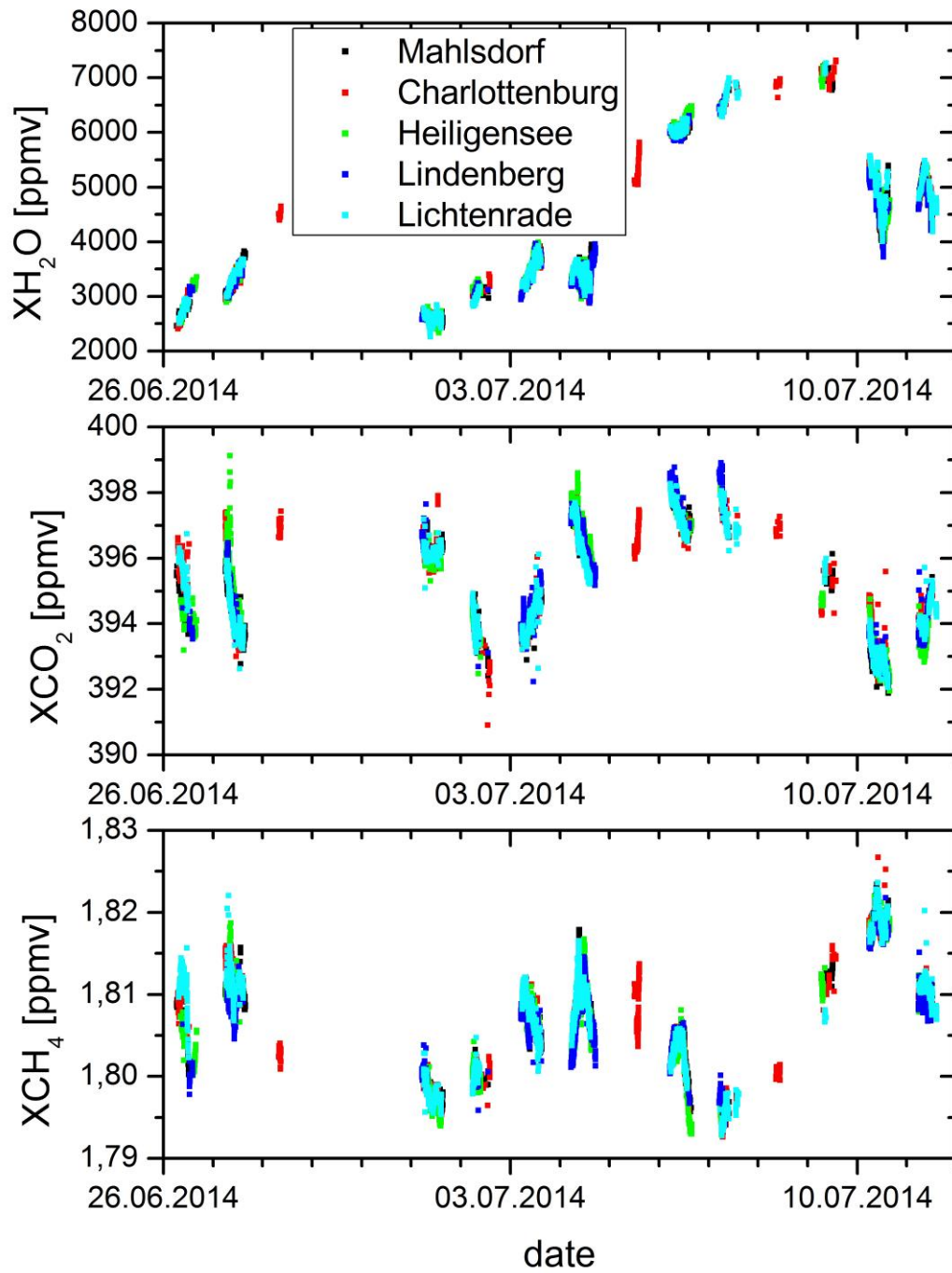
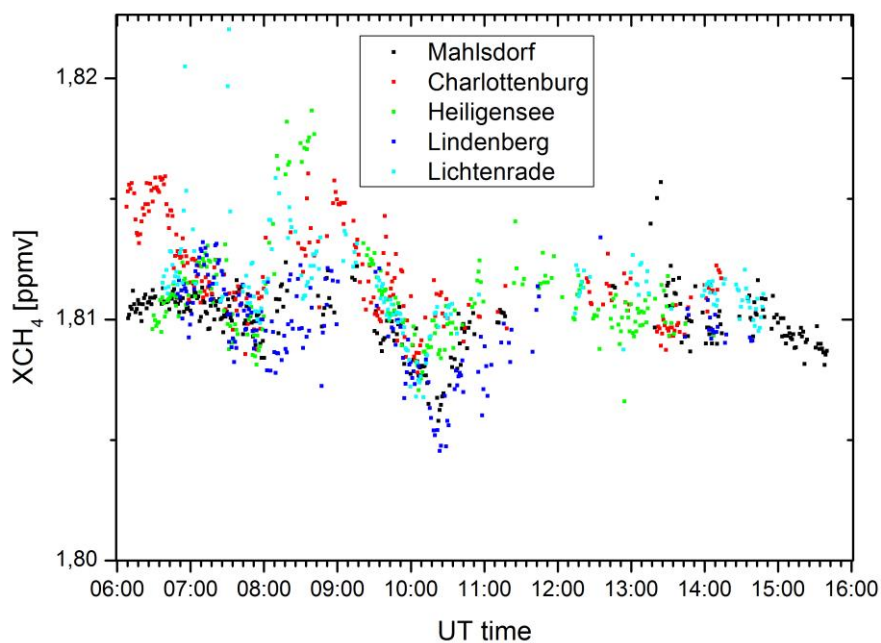
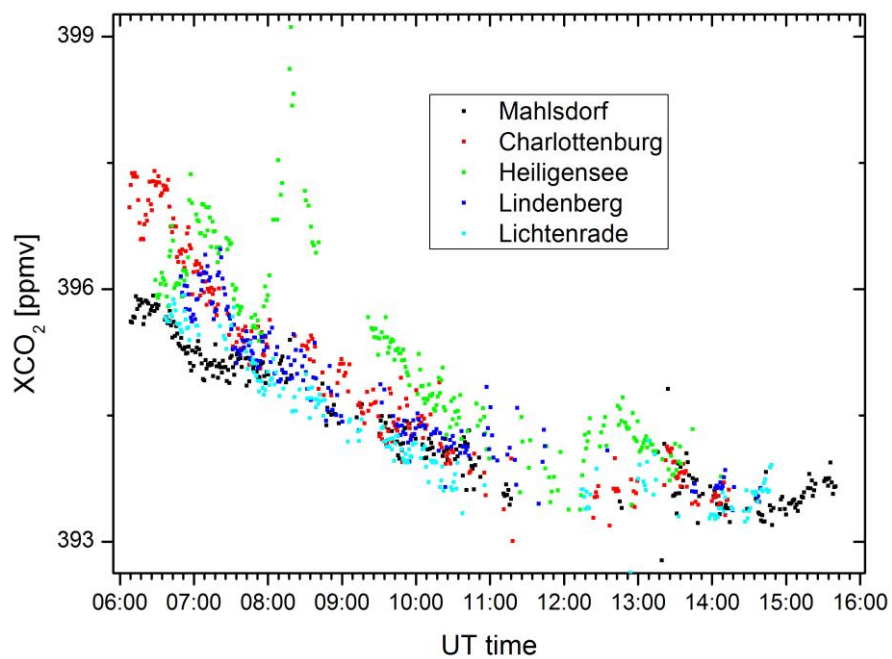


Figure 4. Evolution of XH_2O (top panel), CO_2 (middle panel), and XCH_4 (bottom panel) as measured at all sites during the campaign.



1



2

3 Figure 5. Observed variability of XCH_4 and XCO_2 during 2014-June-27.

4

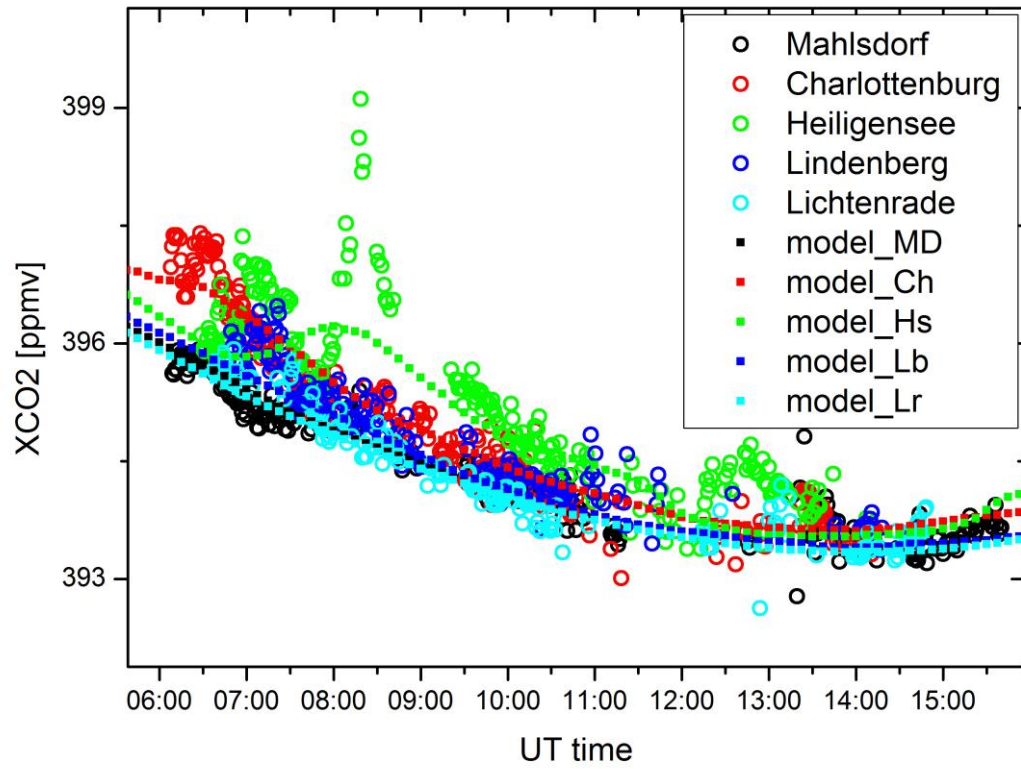


Figure 6. Observed and modelled XCO_2 for June, 27. The model enhancements are shown superimposed on a smooth polynomial background which has been derived from the observations of the upstream stations.

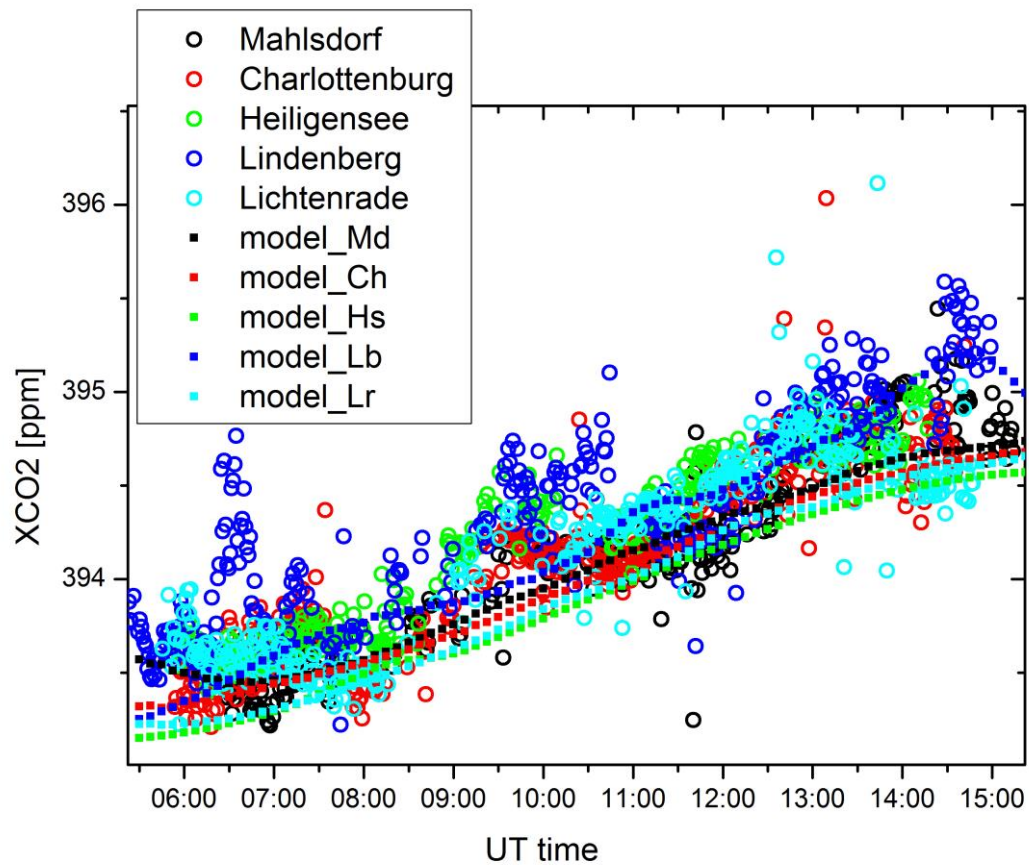
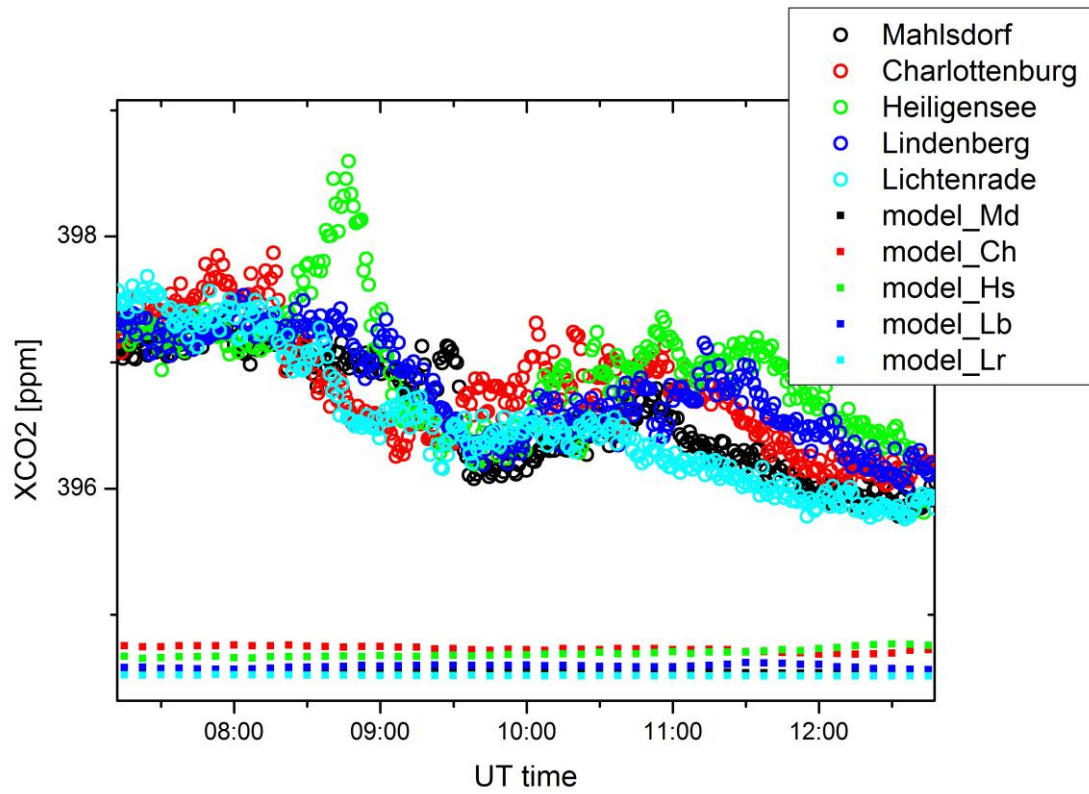
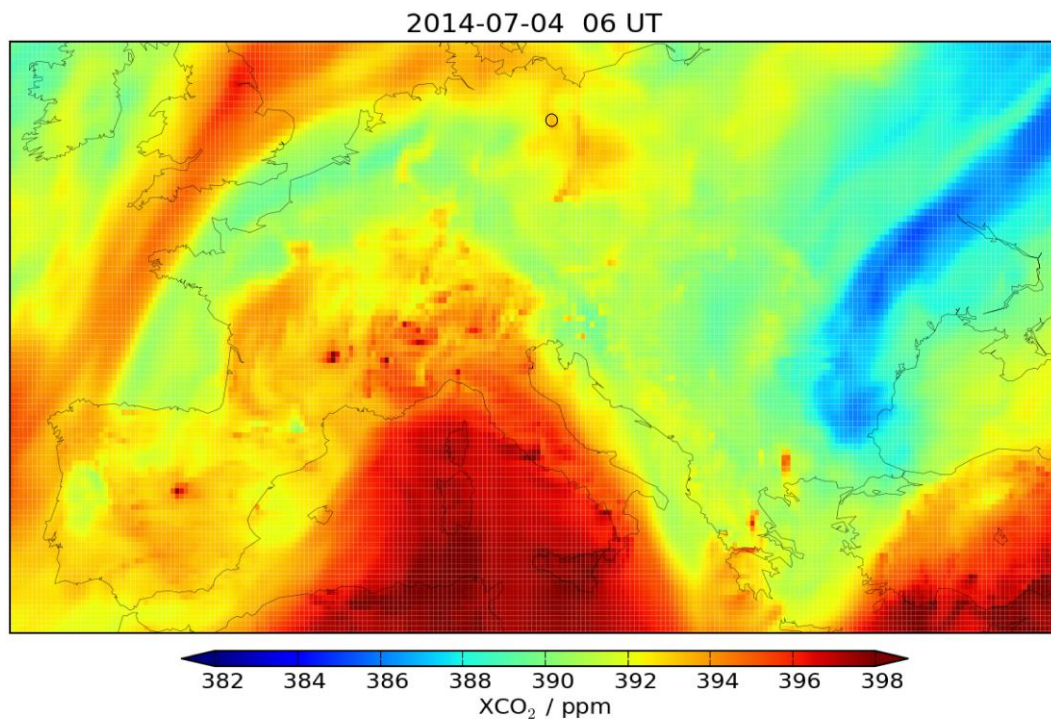


Figure 7. Observed and modelled XCO₂ for July, 3. The model enhancements are shown superimposed on a smooth polynomial background which has been derived from the observations of the upstream stations.



1
2 Figure 8. Observed and modelled XCO₂ for July, 4. Due to the high variability of the
3 upstream values observed during this day, no attempt has been made of constructing a
4 common background value.
5



1
2 Figure 9. XCO₂ distribution according to the MACC model across central Europe for the
3 morning of July, 4. North is up, as orientation marks the continental coastlines are
4 superimposed (dark lines). The open circle denotes the location of Berlin.
5